

Durham Research Online

Deposited in DRO:

13 September 2019

Version of attached file:

Published Version

Peer-review status of attached file:

Peer-reviewed

Citation for published item:

Ludlow, Aaron D and Schaye, Joop and Schaller, Matthieu and Richings, Jack (2019) 'Energy equipartition between stellar and dark matter particles in cosmological simulations results in spurious growth of galaxy sizes.', *Monthly notices of the Royal Astronomical Society : letters.*, 488 (1). L123-L128.

Further information on publisher's website:

<https://doi.org/10.1093/mnrasl/slz110>

Publisher's copyright statement:

This article has been accepted for publication in *Monthly Notices of the Royal Astronomical Society: Letters* ©: 2019 The Authors. Published by Oxford University Press on behalf of the Royal Astronomical

Additional information:

Use policy

The full-text may be used and/or reproduced, and given to third parties in any format or medium, without prior permission or charge, for personal research or study, educational, or not-for-profit purposes provided that:

- a full bibliographic reference is made to the original source
- a [link](#) is made to the metadata record in DRO
- the full-text is not changed in any way

The full-text must not be sold in any format or medium without the formal permission of the copyright holders.

Please consult the [full DRO policy](#) for further details.



Energy equipartition between stellar and dark matter particles in cosmological simulations results in spurious growth of galaxy sizes

Aaron D. Ludlow¹,[★] Joop Schaye²,³ Matthieu Schaller² and Jack Richings^{3,4}

¹International Centre for Radio Astronomy Research, University of Western Australia, 35 Stirling Highway, Crawley, WA 6009, Australia

²Leiden Observatory, Leiden University, PO Box 9513, NL-2300 RA Leiden, the Netherlands

³Institute for Computational Cosmology, Department of Physics, University of Durham, South Road, Durham DH1 3LE, UK

⁴Institute for Particle Physics Phenomenology, Department of Physics, University of Durham, South Road, Durham DH1 3LE, UK

Accepted 2019 July 9. Received 2019 June 17; in original form 2019 March 24

ABSTRACT

The impact of 2-body scattering on the innermost density profiles of dark matter haloes is well established. We use a suite of cosmological simulations and idealized numerical experiments to show that 2-body scattering is exacerbated in situations where there are two species of unequal mass. This is a consequence of mass segregation and reflects a flow of kinetic energy from the more to less massive particles. This has important implications for the interpretation of galaxy sizes in cosmological hydrodynamic simulations, which nearly always model stars with less massive particles than are used for the dark matter. We compare idealized models as well as simulations from the EAGLE project that differ only in the mass resolution of the dark matter component, but keep subgrid physics, baryonic mass resolution, and gravitational force softening fixed. If the dark matter particle mass exceeds the mass of stellar particles, then galaxy sizes – quantified by their projected half-mass radii, R_{50} – increase systematically with time until R_{50} exceeds a small fraction of the redshift-dependent mean interparticle separation, $l(R_{50} \gtrsim 0.05 \times l)$. Our conclusions should also apply to simulations that adopt different hydrodynamic solvers, subgrid physics, or adaptive softening, but in that case may need quantitative revision. Any simulation employing a stellar-to-dark matter particle mass ratio greater than unity will escalate spurious energy transfer from dark matter to baryons on small scales.

Key words: methods: numerical – galaxies: formation – dark matter.

1 INTRODUCTION

Cosmological simulations of collisionless dark matter (DM) make reliable predictions for the innermost structure of DM haloes. Such simulations incur relatively modest computational cost and have been repeated at ever increasing resolution, exposing the limits of their reliability (see e.g. Stadel et al. 2009; Navarro et al. 2010). Controlling for other numerical parameters – such as time-stepping, integration accuracy, and gravitational softening – their main impediment is 2-body relaxation, which sets a lower limit to the spatial resolution of any N -body simulation (Power et al. 2003; hereafter P03; Ludlow, Schaye & Bower 2019; hereafter LSB19). This limitation is well understood and readily accounted for, leading to widespread agreement on the innermost structure of DM haloes.

Such simulations provide the rudimentary infrastructure for modelling galaxy formation, offering a tangible connection to observational astrophysics. Current approaches to this problem follow semi-analytic or halo occupation methods – here the physics

of galaxy formation is divorced from the evolution of DM – or simultaneously model the co-evolution of DM and baryonic fluids. In both approaches, subresolution models for galaxy formation require calibration against observables before sensible predictions for galaxy populations can be made. This may overshadow the complex non-linear coupling between numerical and subgrid parameters, and may mask subtle numerical effects.

One possible issue – which we highlight in this letter – is the importance of 2-body relaxation for the *stellar* component of simulated galaxies. Stars are treated as collisionless particles in cosmological simulations and, like DM, their dynamics must be subject to 2-body scattering. Galaxies formed in cosmological simulations, while calibrated to resemble observed systems, may therefore evolve in a way that is subject to numerical artefact.

In Section 2 we discuss the importance of 2-body scattering in N -body simulations, emphasizing differences between uniform resolution runs and those involving mixtures of DM and stars of unequal mass, which is the conventional approach. We present simple numerical experiments that illustrate the effects. In Section 3.1 we describe the cosmological simulations used to test the impact of 2-body scattering on the evolution of stellar systems; their results

* E-mail: aaron.ludlow@icrar.org

are presented in Sections 3.2 and 3.3. We provide some closing remarks in Section 4.

2 2-BODY RELAXATION IN AN IDEALIZED GALAXY-HALO MODEL

Cosmological simulations involve mixtures gas, stars, and DM particles typically of unequal mass. When collisions cannot be ignored, their evolution is subject to 2-body scattering and, when masses are unequal, to energy equipartition (e.g. Spitzer & Hart 1971). The net energy exchange between species due to these processes can be described by a diffusion equation, with coefficients that depend on their initial phase-space distributions, and the ratio of particle masses.

Following Binney & Tremaine (2008), we consider the collisional relaxation time of such a system, neglecting the gas component. We define the particle mass ratio, $\mu \equiv m_1/m_2 \geq 1$, and the fraction of mass in m_2 : $\psi \equiv M_2/M_1 = N_2 m_2/N_1 m_1$, where N_i are the number of particles of species i . A test particle that traverses a system of size R will experience $\delta n = \delta n_1 + \delta n_2 \approx 2\pi (\Sigma_1 + \Sigma_2) b db$ collisions with impact parameters in the range $(b, b + db)$, where $\Sigma_1 = N_1/\pi R^2$ and $\Sigma_2 = \psi \mu N_1/\pi R^2$ are the surface densities of species 1 and 2, respectively. From the impulse approximation, any single encounter results in a small velocity perturbation ($\delta v \ll v$) perpendicular to the particle's direction of motion; its trajectory is unaltered. Regardless of its mass, velocity perturbations are of order $|\delta v_i| \approx 2G m_i/(b v)$ for encounters with particles of mass m_i . Such encounters add incoherently and their cumulative effect will be given by integrating $\delta v_i^2 \delta n_i + \delta v_j^2 \delta n_j$ over some range of impact parameters, b_{\min} to b_{\max} . The relative square velocity change after traversing the system is given by

$$\frac{\Delta v^2}{v^2} = \frac{8}{N_1} \ln \Lambda \frac{(1 + \psi/\mu)}{(1 + \psi)^2}, \quad (1)$$

where we have assumed a typical velocity $v^2 \approx G N_1 m_1 (1 + \psi)/R$, and $\Lambda \equiv b_{\max}/b_{\min}$ is the Coulomb logarithm.

For cosmological simulations equation (1) can be simplified if we identify species 1 with DM and species 2 with stars; ψ is then the stellar-to-DM halo mass ratio, typically $\lesssim 0.05$. Assuming equal numbers of baryon and DM particles $\mu = (\Omega_M - \Omega_{\text{bar}})/\Omega_{\text{bar}}$, where Ω_M and Ω_{bar} are the cosmic densities of matter and baryons, respectively. In this case $\mu \geq 1$ and $\psi \ll 1$, and the ratio of bracketed terms in equation (1) is close to unity and may be ignored. If we further assume $b_{\max} = R$ and set $b_{\min} = b_{90} = G(m_1 + m_2)/v^2$ as the impact parameter yielding 90° deflections, then $\Lambda = N_1(1 + \psi)/(1 + \mu^{-1}) \approx N_1$ and equation (1) reduces to $\Delta v^2/v^2 \approx 8 \ln N_1/N_1$. The relaxation of *both* species is driven by encounters with *massive* particles.

The number of orbits a particle must complete so that $\Delta v^2/v^2 \approx 1$ defines the relaxation time, $t_{\text{rel}} = t_{\text{orb}}/(\Delta v^2/v^2)$. In units of the Hubble time (roughly the orbital time at the radius,¹ r_{200}), $t_H \approx 2\pi r_{200}/V_{200}$, this can be expressed

$$\kappa_{\text{rel}} \equiv \frac{t_{\text{rel}}}{t_H} = \frac{N_1}{8 \ln N_1} \frac{t_{\text{orb}}}{t_H} = \frac{\sqrt{200}}{8} \frac{N_1}{\ln N_1} \left(\frac{\bar{\rho}}{\rho_{\text{crit}}} \right)^{-1/2}, \quad (2)$$

¹We define r_{200} as the size of a sphere centred on the particle with the minimum potential energy that encloses a mean density of $200 \times \rho_{\text{crit}}$, where $\rho_{\text{crit}}(z) = 3H(z)^2/(8\pi G)$ is the critical density. The corresponding mass is $M_{200} = (800/3)\pi r_{200}^3 \rho_{\text{crit}}$ and circular velocity, $V_{200} = \sqrt{GM_{200}/r_{200}}$.

where $N \equiv N(r)$ is the enclosed particle number, $\bar{\rho}(r)$ the enclosed density, and $t_{\text{orb}} = 2\pi r/V$ is the local orbital time² (P03). When other numerical parameters are chosen wisely, t_{rel} sets a minimum resolved spatial scale within which collisions cannot be ignored. The solution to equation (2) thus defines a ‘convergence radius’, r_{conv} , which marks the location at which $\kappa_{\text{rel}} \sim 1$ (see e.g. P03; LSB19).

The value of κ_{rel} corresponding to a certain level of convergence must be obtained empirically by comparing simulations of differing mass resolution. P03 found that, for DM-only simulations, the circular velocity profile, $V_c(r)$, of an individual Milky Way-mass halo converges to ≈ 10 per cent at the radius where $\kappa \approx 0.6$; similar convergence in the *average* $V_c(r)$ profiles requires a less conservative value, $\kappa \approx 0.18$, regardless of halo mass (LSB19). A convenient approximation is given by $r_{\text{conv}} = 0.174 \kappa_{\text{rel}}^{2/3} l$, where $l = L_{\text{box}}/N_{\text{part}}^{1/3}$ is the mean interparticle spacing in physical units, and $\kappa_{\text{rel}} = 0.18$ (LSB19).

When $\mu \neq 1$, 2-body collisions also lead to a *segregation* of the two components: massive particles will, on average, lose energy to less massive ones, causing them to congregate in halo centres while heating the low-mass component. This ‘mass segregation’ signals the onset of energy equipartition.

The simple two-component toy model of Spitzer (1969) suggests that the segregation time-scale, t_{seg} , is shorter than t_{rel} by a factor roughly equal to the ratio of the particle masses:

$$t_{\text{seg}} = \frac{t_{\text{rel}}}{\mu} \approx \frac{N_1}{8 \ln N_1} \frac{t_{\text{orb}}}{\mu}. \quad (3)$$

Homogeneous mixtures of particles of different mass will therefore segregate at radii $r_{\text{seg}} \geq r_{\text{conv}}$ provided $\mu \geq 1$. A simple estimate of r_{seg} therefore follows from equation (2) (or from $r_{\text{conv}} = 0.174 \kappa_{\text{rel}}^{2/3} l$) if κ_{rel} is replaced by $\kappa_{\text{seg}} = \mu \kappa_{\text{rel}}$. Whether equipartition can be reached, however, depends on the ratios of particle mass, μ , and of the total mass of each component, M_1/M_2 , and r_{seg} should therefore be viewed as an upper limit. (Simple analytic estimates and numerical results suggest that full equipartition may not be possible if $M_1 \gtrsim M_2 \mu^{-3/2}$, which is almost always the case in DM-dominated galaxies.)

As $\mu \rightarrow 1$, the importance of mass segregation diminishes. Nevertheless, different species may still structurally evolve through 2-body scattering and, as we show below, this evolution is sensitive to the *initial* segregation of each component. (The sensitivity to initial segregation becomes clear when comparing the idealized tests presented in Fig. 1 to the collisionless cosmological runs in Fig. 2, which start with both species equally mixed).

Fig. 1 shows results from numerical experiments designed to illustrate these effects. We consider here idealized equilibrium systems composed of a galaxy embedded within a DM halo. Both are modelled as spherical, collisionless Hernquist (1990) spheres with galaxy-to-halo mass ratio $M_{\text{gal}}/M_h = 0.027$ (close to the ‘peak’ galaxy formation efficiency of Behroozi, Wechsler & Conroy 2013) and ratio of scale radii $r_{\text{half}}/a_h = 0.25$ (r_{half} and a_h are the galaxy half-mass radius and halo scale radius, respectively). Initial conditions, constructed using GALIC (Yurin & Springel 2014), differ only in the stellar-to-DM particle mass ratio, μ . GALIC assigns particle phase-space coordinates iteratively in order to optimally match an

²A more common definition of the relaxation time is based on the number of *crossings* a particle must execute such that $\Delta v^2/v^2 \approx 1$, which differs from our definition by a factor $t_{\text{orb}}/t_{\text{cross}} = \pi$. We adopt the orbital time to define t_{rel} for consistency with P03: in this case, $t_{\text{orb}}/t_H \approx (r/V)/(r_{200}/V_{200})$ results in equation (2).

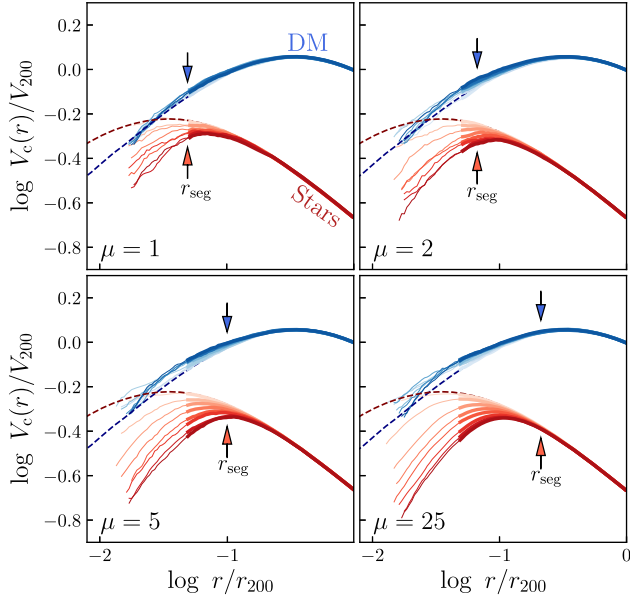


Figure 1. Circular velocity profiles of DM (blue lines) and stars (red lines) in a set of idealized numerical simulations starting from equilibrium initial conditions (dashed curves). The DM halo is sampled with $N_1 = 5 \times 10^4$ particles; the stellar component, also modelled using collisionless particles, has a mass fraction of 2.7 per cent of the system’s total mass, but a total number of particles $N_2 \propto \mu N_1$, where $\mu = 1, 2, 5$, and 25 (top to bottom, left to right). Different tints and shades correspond to earlier and later outputs of the simulation, respectively, which are spaced linearly from $t = 0$ to $t \approx 13.3$ Gyr. For individual profiles, the thick lines extend to the convergence radius dictated by 2-body relaxation (equation 2, with $\kappa_{\text{rel}} = 0.6$), and arrows mark the radius r_{seg} (equation 3).

underlying analytic distribution function, which is itself a stable solution to the collisionless Boltzmann equation and therefore in collisionless equilibrium.³ We adopt $N_1 = 5 \times 10^4$ (for DM), and consider $\mu = 1, 2, 5$, and 25. All runs used the same softening length, $\epsilon/l_h = 0.1$ ($l_h = [3/4\pi N_1]^{1/3}$ is the Wigner–Seitz radius), and were evolved using GADGET-2 (Springel 2005) for $t \approx 13.3$ Gyr. (We have verified that our simulation results are robust to small changes in time-stepping and softening length.) Because these systems are initially in collisionless equilibrium, any evolution away from the initial state must be driven by 2-body scattering.

Different panels correspond to different μ , as indicated. Solid blue curves show $V_{c,1}(r)$ for the DM, and solid red curves show $V_{c,2}(r)$ for stars; tints and shades encode the time evolution, which increases linearly from $t = 0$ (light) to $t \approx 13.3$ Gyr (dark). Dashed lines of corresponding colour show the initial profiles used to construct the galaxy/halo models. For each curve (except the initial profiles) thick lines extend down to the convergence radius expected from equation (2) (for $\kappa_{\text{rel}} = 0.6$); thin lines extend to the radius enclosing 100 DM particles.

DM profiles are reasonably stable for $r \gtrsim r_{\text{conv}}$, as is the case for stars if $\mu = 1$. Note, however, that as μ increases, the curves deviate systematically from their initial profile at radii $\gtrsim r_{\text{conv}}$; this

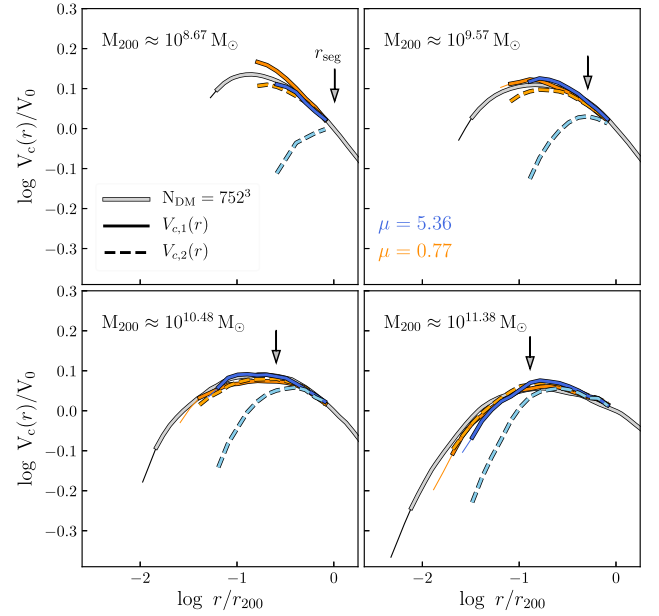


Figure 2. Median ($z = 0$) circular velocity profiles of DM haloes in simulations of collisionless particle mixtures. Different panels correspond to different masses, M_{200} , which increase from $M_{200} = 10^{8.5} M_\odot$ by successive factors of 8 between panels. Blue curves correspond to the run with $N_{\text{DM}} = N_{\text{gas}} = 188^3$ ($\mu = 5.36$); orange curves to the one with $N_{\text{gas}} = 188^3$ and $N_{\text{DM}} = 7 \times 188^3$ ($\mu = 0.77$). Solid curves represent DM particles whereas dashed curves represent ‘gas’ particles. Grey curves correspond to the median $V_c(r)$ profiles of haloes in our single-component DM-only run carried out with $N_{\text{part}} = 752^3$ particles. For all profiles we use thick line segments for $r > 0.055 l$ and thin lines extend to the P03 convergence radius ($\kappa = 0.6$). Downward pointing arrows denote the radius $r_{\text{seg}} = 0.055 \mu^{2/3} l$, below which we expect substantial segregation of DM and ‘gas’ particles in the $\mu = 5.36$ run.

is particularly true for stars. The arrows mark r_{seg} calculated from equation (2) after replacing t_{rel} by $t_{\text{seg}} = t_{\text{rel}}/\mu$. For $\mu \lesssim 5$, these arrows track more closely the radii at which $V_c(r)$ profiles first show noticeable differences from their initial values. Note also that the segregation of the stars and DM is much more prominent when μ is large: DM haloes develop denser centres while the stellar component gradually expands. Importantly, even for $\mu = 1$ there is considerable evolution in $V_{c,2}(r)$ for $r \lesssim r_{\text{conv}}$. This is because 2-body collisions will tend to homogenize populations that are initially segregated. 2-body scattering can be thought of as a diffusion process with different coefficients describing the first- and second-order processes. For particular initial configurations – which depend on μ , M_1/M_2 , and the spatial segregation of each species – energy equipartition may give rise to mass segregation. For the particular case of $\mu = 1$ the diffusion coefficients are equal, and 2-body scattering will lead to a *mixing* of the two components. In that case, a centrally compact stellar component will tend to become more diffuse with time, as seen in the upper left panel of Fig. 1, even if it was *constructed* to be in collisionless equilibrium initially (note that scattering-driven diffusion is largely confined to within the convergence radius, as expected for $\mu = 1$).

3 COSMOLOGICAL SIMULATIONS

3.1 Simulation set-up

DM haloes and their associated galaxies form hierarchically through accretion and mergers and are, at best, *quasi*-equilibrium structures.

³We have verified that GalICs yields stable particle configurations for our experiments by carrying out tests for which $\mu = 1$ (to eliminate mass segregation) and $N_1 = 10^6$ (to suppress 2-body scattering). Our tests confirm that the mass profiles of species 1 and 2 remain stable at $r \gtrsim r_{\text{conv}}$ for a Hubble time.

Table 1. Basic numerical parameters used for our cosmological simulations. N_1 refers to the number of ‘dark matter’ particles of species 1; N_2 to the number of ‘gas’ particles, species 2. The corresponding particles masses are m_1 and m_2 , respectively, and their ratio is denoted $\mu \equiv m_1/m_2$; L_{box} is the simulation box size. The run type is also provided: DMO refers to runs for which both species were assumed to be collisionless particles, and ‘EAGLE’ refers to hydrodynamical runs carried out using the Reference model of the EAGLE project.

N_1	N_2	m_1 ($10^5 M_\odot$)	m_2 ($10^5 M_\odot$)	μ	L_{box} (Mpc)	Type
752^3	0	1.8	0	–	12.5	DMO
188^3	188^3	97.0	18.1	5.36	12.5	DMO
7×188^3	188^3	13.9	18.1	0.77	12.5	DMO
376^3	376^3	97.0	18.1	5.36	25.0	EAGLE
7×376^3	376^3	13.9	18.1	0.77	25.0	EAGLE

It is therefore worthwhile to test the importance of mass segregation and 2-body scattering in cosmological simulations that include two particle species. The remainder of the paper will focus on such simulations.

All cosmological runs used parameters consistent with the Planck Collaboration XVI (2014) data release: $h \equiv H_0/(100 \text{ km s}^{-1} \text{ Mpc}^{-1}) = 0.6777$ is the Hubble parameter; $\sigma_8 = 0.8288$ the ($z = 0$) rms density fluctuation in $8 h^{-1} \text{ Mpc}$ spheres; and $\Omega_M = 1 - \Omega_\Lambda = 0.307$ and $\Omega_{\text{bar}} = \Omega_M - \Omega_{\text{DM}} = 0.04825$, are the energy density parameters in units of ρ_{crit} .

We use three cosmological simulations that echo those used by Binney & Knebe (2002) to investigate 2-body scattering in cosmological DM-only simulations. The first evolves the DM with $N_{\text{part}} = 752^3$ equal-mass particles ($m_{\text{DM}} = 1.8 \times 10^5 M_\odot$). The second uses two particle species of equal abundance, $N_1 = N_2 = 188^3$, but with a mass ratio $\mu = \Omega_{\text{DM}}/\Omega_{\text{bar}} \approx 5.36$; this run is analogous to most cosmological hydrodynamical simulations (DM and baryons are sampled with equal particle numbers) but differs by modelling both species as collisionless fluids. The masses of DM (species 1) and ‘gas’ particles (species 2) are, respectively, $m_{\text{DM}} = 97.0 \times 10^5 M_\odot$ and $m_{\text{gas}} = 18.1 \times 10^5 M_\odot$. The final run also adopts a two collisionless components, but with unequal particle numbers: $N_1/7 = N_2 = 188^3$ and hence $\mu = (1/7) \Omega_{\text{DM}}/\Omega_{\text{bar}} \approx 0.77$ (or $m_{\text{DM}} = 13.9 \times 10^5 M_\odot$). Initial conditions were created from those described above by splitting DM particles into seven equal-mass particles and arranging them on a cubic lattice in a manner that preserves a force-free unperturbed particle load. All runs used a linear box size of $L_{\text{box}} = 12.5 \text{ Mpc}$ (comoving) and identical phases and amplitudes for mutually resolved modes. They differ only in the number of particles of species 1, and hence in μ .

The particle mixture models were repeated for the second set of simulations (in a larger volume; $L_{\text{box}} = 25 \text{ Mpc}$) but with species 2 treated as a gaseous fluid ($N_{\text{gas}} = N_2 = 376^3$). These runs employ cooling, star formation, and feedback from stars and active galactic nuclei in accord with the Reference model of the EAGLE program (see Schaye et al. 2015). They differ only in the number of DM particles: one has $N_{\text{DM}} = N_{\text{gas}} = 376^3$ ($\mu \approx 5.36$) and the other $N_{\text{DM}} = 7 \times N_{\text{gas}} = 7 \times 376^3$ ($\mu = 0.77$). At $z = 0$, star particles have an average mass of roughly 65 percent of the primordial gas particle mass (stars lose mass to gas particles through stellar winds as they evolve). As a result, $\mu_* \equiv m_{\text{DM}}/m_* \approx 1.18$ in our runs, but we neglect this small departure from unity. The main numerical aspects of our cosmological simulations are provided in Table 1.

All runs used the same softening length for both species, which is a fixed fraction of the mean baryonic interparticle separation:⁴ $\epsilon/l = 0.04$ (comoving) for $z > 2.8$, and $\epsilon/l = 0.01$ (physical) thereafter. Haloes were identified using SUBFIND (Springel et al. 2001), which returns the coordinate of the particle with the minimum potential energy, \mathbf{x}_{MB} , as well as r_{200} , M_{200} , and V_{200} .

As in Fig. 1, we focus our analysis on the circular velocity profiles of each mass component, and use subscripts to denote the relevant species. (For example, $V_{c,1}(r)$ refers to the circular velocity profile of particles of mass m_1 .) Hereafter, for clarity, we drop explicit reference to DM or baryonic particles, even in the hydrodynamic runs, but instead identify DM with species 1 and stars with species 2. We do not consider the mass profiles of gas particles in our hydrodynamic simulations.

3.2 Cosmological simulations with unequal-mass collisionless particles

Fig. 2 shows the median ($z = 0$) circular velocity profiles of haloes in four separate mass bins in our collisionless cosmological runs. Grey curves correspond to the uniform resolution ($N_{\text{part}} = 752^3$) simulation, which can be used to assess convergence in the lower resolution runs. Blue curves correspond to the run with $N_1 = N_2 = 188^3$ ($\mu = 5.36$); orange to the one with $N_1/7 = N_2 = 188^3$ ($\mu = 0.77$). Thick lines extend down to $r_{\text{conv}} = 0.055 l$ (LSB19), where l is the mean interparticle spacing⁵ of particles of mass m_1 ; thin lines to the r_{conv} expected from equation (2) with $\kappa_{\text{rel}} = 0.6$. To aid the comparison, all curves have been normalized to $V_0 = \sqrt{G M_{200,i}/r_{200}}$, where $M_{200,i}$ is the mass of species i enclosed by r_{200} .

This figure prompts a few comments. First, notice that, for simulations involving particle mixtures, the $V_{c,1}(r)$ profiles agree reasonably well with those of equal-mass haloes in the uniform resolution run (the solid coloured curves align closely with the grey curves). The largest differences in $V_c(r)$ are $\lesssim 10$ per cent for $r > r_{\text{conv}}$, as expected. Particles of mass m_2 , however, behave differently depending on μ . For $\mu \approx 0.77$ (dashed orange lines), the circular velocity profiles of species 1 and 2 are similar: both deviate by $\lesssim 10$ per cent from the high-resolution run for all $r > r_{\text{conv}}$ and all halo masses considered. This is expected: since μ is close to 1, and both species are initially well mixed, it follows that $t_{\text{seg}} \approx t_{\text{rel}}$ and $r_{\text{seg}} \approx r_{\text{conv}}$, and both species should remain approximately homogeneous at $r \gtrsim r_{\text{conv}}$ at all times. For $\mu \approx 5.36$, however, this is not the case: for $r \lesssim r_{\text{seg}}$, $V_{c,2}(r)$ is considerably lower than what is expected for a purely collisionless system, consistent with mass segregation driven by 2-body scattering (this confirms the results of Binney & Knebe 2002). The radius below which this suppression becomes significant coincides roughly with r_{seg} (downward pointing arrows), approximated by $r_{\text{seg}} = 0.174 (\mu \kappa_{\text{rel}})^{2/3} l \approx 3.1 r_{\text{conv}}$ (assuming $\kappa_{\text{rel}} = 0.188$; LSB19).

3.3 Impact of 2-body scattering on galaxy sizes

Many cosmological simulations spawn one star particle per gas particle, which typically have comparable masses but are $\approx \Omega_{\text{bar}}/(\Omega_M - \Omega_{\text{bar}})$ times less massive than the DM particles. Other simulations

⁴For $N_p = 752^3$, we use the DM interparticle spacing.

⁵If we were to use instead $l = L_{\text{box}}/N_{\text{tot}}$, where $N_{\text{tot}} = N_1 + N_2$, r_{conv} would be smaller by a factor of $2^{1/3} \approx 1.26$. This will not affect the interpretation of our results, so we opt for the more conservative estimate of r_{conv} .

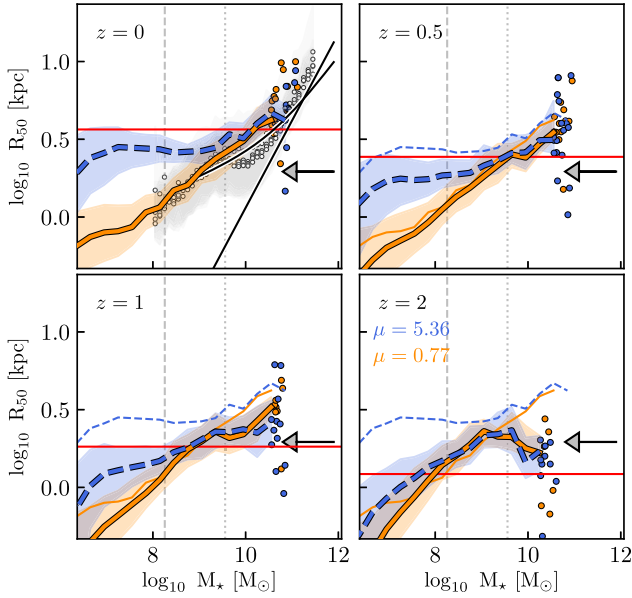


Figure 3. Projected half-mass radius as a function of stellar mass at $z = 0, 0.5, 1$, and 2 . Dashed (blue) lines correspond to $\mu = m_{\text{DM}}/m_{\text{gas}} = 5.36$ and solid (orange) lines to $\mu = 0.77$. Thin lines, repeated in all panels, show the $z = 0$ relations for comparison. The vertical dashed and dotted lines indicate the mass scales of 100 and $2000 \times m_{\text{gas}}$, respectively; red lines mark r_{conv} for the DM component of the $\mu = 5.36$ run; arrows mark the spline softening lengths, $2.8 \times \epsilon$, above which gravitational forces are exactly Newtonian. The much stronger evolution of R_{50} when $\mu = 5.36$ is due to numerical mass segregation. For comparison, we plot circularized half-light radii for early- and late-type galaxies in SDSS (thick black line; Shen et al. 2003) and GAMA (points; Lange et al. 2015) at $z=0$.

attempt to increase the resolution of the stellar component by generating multiple star particles per gas particle which are considerably less massive (e.g. Dubois et al. 2014; Revaz & Jablonka 2018). Galaxies formed in both types of simulations may be subject to equipartition effects, which may have important implications for the interpretation of galaxy sizes, among other properties.

What impact does equipartition have on galaxy sizes in cosmological hydrodynamical simulations? Fig. 3 summarizes the results of our tests. Each panel shows the median projected half-stellar mass radii, R_{50} , as a function of galaxy stellar mass (masses are defined using bound stellar particles within a 100 physical kpc aperture centred on \mathbf{x}_{MB}) at four different redshifts: $z = 0, 0.5, 1$, and 2 . We use blue curves for $\mu = 5.36$ and orange curves for $\mu = 0.77$. The vertical dashed lines correspond to 100 primordial gas particles, dotted lines to 2000 . These runs use identical baryonic mass resolution, force softening (arrows indicate $2.8 \times \epsilon$) and subgrid physics models; they differ *only* in DM particle mass.

Galaxy sizes show clear differences between these runs, both in their mass and redshift dependence. Consider first $z = 0$ (upper left panel). For $\mu = 5.36$, the median size–mass relation flattens abruptly for stellar masses $M_* \lesssim 2000 m_{\text{gas}}$ (dotted vertical line) below which $R_{50} \approx 2.8$ kpc, regardless of M_* . For $\mu \approx 0.77$ this is not observed: sizes continue to decrease monotonically with decreasing M_* to the lowest mass-scale considered (≈ 10 stellar particles). Similar results are seen at $z = 0.5$ for $\mu = 5.36$, although in this case R_{50} levels-off at lower mass ($M_* \approx 10^{8.7} M_{\odot}$), and correspondingly smaller size ($R_{50} \approx 2$ kpc). For $\mu = 0.77$ galaxy sizes evolve very little from $z = 0.5$ to $z = 0$ (thin lines, repeated in all panels, show the $z = 0$ size–mass relations for comparison).

Note as well that, for the different μ values, sizes begin to converge at higher redshift: by $z = 2$, for example, they are virtually indistinguishable for galaxies resolved with more than ≈ 100 particles. Intriguingly, convergence is attained at all z provided sizes exceed the physical convergence radius of haloes in the $\mu = 5.36$ run (shown here as $r_{\text{conv}} = 0.055 l$ and highlighted using a red horizontal line; see LSB19).

Although using $\mu \approx 1$ will minimize the spurious transport of energy between particle species, we emphasize that by itself it does not guarantee that the simulations are immune to numerical effects. Convergence tests that simultaneously increase both the DM and baryonic resolution, and use $\mu \approx 1$, are required to test in which regime the results are robust.

4 SUMMARY AND DISCUSSION

Previous studies of galaxy sizes in cosmological simulations report trends similar to those in Fig. 3 for $\mu = 5.36$. In EAGLE, Furlong et al. (2017) note that galaxy sizes increase systematically with increasing M_* and with decreasing redshift. They identified a sample of passive galaxies between $z = 1.5$ and 2 that remain quiescent centrals until $z = 0$: all grow in size between their identification redshift and $z = 0$. They report that compact centrals at $z = 2$ grow secularly by ‘stellar migration’ to the present day.

Campbell et al. (2017) present convergence tests of projected half-mass radii in the Apostle simulations (Sawala et al. 2016, $\mu \approx 5.36$). Comparing low-, intermediate-, and high-resolution runs they show that R_{50} flattens at a characteristic scale comparable to the spline softening length. Our results indicate that sizes are subject to spurious growth below scales comparable to the convergence radius ($\approx 0.055 l$) which are close to those quoted by Campbell et al. (2017). We can distinguish between softening and 2-body scattering as the culprit for this resolution dependence using the redshift evolution of R_{50} . If softening is the cause, then $R_{50} \approx \epsilon$ should set the minimum size *at all redshifts*, whereas 2-body scattering would give rise to a *slow growth* of R_{50} for poorly resolved galaxies. Our results support the latter explanation (Fig. 3).

Similar results were recently reported for galaxy sizes in the Illustris TNG50 simulation (Pillepich et al. 2019). In TNG50, for which $\mu \approx 5.3$, the sizes of low-mass galaxies flatten at systematically larger physical scales, and at higher stellar masses, as mass-resolution decreases. These results are *not* consistent with softening setting a minimum physical size to low-mass galaxies. In TNG100, Genel et al. (2018) also report a flattening of sizes for low-mass galaxies, an effect that becomes more pronounced for quiescent systems. They also note that, during quenched phases, galaxy sizes increase systematically with time, particularly among poorer resolved low-mass systems, despite little growth in stellar mass over the same period. The secular growth of sizes of non-star-forming galaxies (e.g. dwarfs or ellipticals) is an *expected consequence* of (spurious) energy equipartition between stellar and DM particles.

Our explanation is that 2-body scattering leads to a slow diffusion of stellar particles out of the dense central regions of galaxies. This is consistent with the simulations of Revaz & Jablonka (2018, $\mu = 21.9$), in which quenched dwarf galaxies grow systematically in size with decreasing z , despite their passive evolution. Indeed, Revaz & Jablonka (2018) hypothesize that this result is due to 2-body scattering.

We note that hydrodynamical simulations involve gas particles that may also be subject to mass segregation if their masses differ from those of the DM, but in this case there is a compounding effect:

collisions with DM particles also tend to *heat* gas particles as the kinetic energy associated with velocity perturbations thermalizes (see Steinmetz & White 1997, for details). Disentangling these effects (mass segregation and gravitational heating) will be challenging, and requires further study.

Finally, we note that assessing the impact of equipartition on galaxy sizes *does not* require time-consuming, high-resolution simulations of large volumes. Since the effect appears limited to haloes/galaxies of relatively low-particle number it can be gauged by comparing runs in relatively small volumes that reach the target stellar mass resolution but vary μ . 2-body scattering may also affect velocity dispersion and anisotropy profiles, angular momentum distributions, and gas fractions. These issues will be addressed in a follow-up paper.

ACKNOWLEDGEMENTS

We thank Adrian Jenkins and Chris Power for useful conversations, and our referee, Alexander Knebe, for a useful report. ADL is supported by the Australian Research Council (project Nr. FT160100250). This work used the DiRAC@Durham facility managed by the Institute for Computational Cosmology on behalf of the STFC DiRAC HPC Facility (www.dirac.ac.uk). The equipment was funded by BEIS capital funding via STFC capital grants ST/K00042X/1, ST/P002293/1, ST/R002371/1, and ST/S002502/1, Durham University and STFC operations grant ST/R000832/1.

REFERENCES

Behroozi P. S., Wechsler R. H., Conroy C., 2013, *ApJ*, 770, 57

- Binney J., Knebe A., 2002, *MNRAS*, 333, 378
 Binney J., Tremaine S., 2008, *Galactic Dynamics*, 2nd edn. Princeton Univ. Press, Princeton, NJ
 Campbell D. J. R. et al., 2017, *MNRAS*, 469, 2335
 Dubois Y. et al., 2014, *MNRAS*, 444, 1453
 Furlong M. et al., 2017, *MNRAS*, 465, 722
 Genel S. et al., 2018, *MNRAS*, 474, 3976
 Hernquist L., 1990, *ApJ*, 356, 359
 Lange R. et al., 2015, *MNRAS*, 447, 2603
 Ludlow A. D., Schaye J., Bower R., 2019, *MNRAS*, in press
 Navarro J. F. et al., 2010, *MNRAS*, 402, 21
 Pillepich et al., 2019, preprint (arXiv:1902.05553)
 Planck Collaboration XVI, 2014, *A&A*, 571, A16
 Power C., Navarro J. F., Jenkins A., Frenk C. S., White S. D. M., Springel V., Stadel J., Quinn T., 2003, *MNRAS*, 338, 14
 Revaz Y., Jablonka P., 2018, *A&A*, 616, A96
 Sawala T. et al., 2016, *MNRAS*, 457, 1931
 Schaye J. et al., 2015, *MNRAS*, 446, 521
 Shen S., Mo H. J., White S. D. M., Blanton M. R., Kauffmann G., Voges W., Brinkmann J., Csabai I., 2003, *MNRAS*, 343, 978
 Spitzer L., Jr., 1969, *ApJ*, 158, L139
 Spitzer L., Jr., Hart M. H., 1971, *ApJ*, 166, 483
 Springel V., 2005, *MNRAS*, 364, 1105
 Springel V., White S. D. M., Tormen G., Kauffmann G., 2001, *MNRAS*, 328, 726
 Stadel J., Potter D., Moore B., Diemand J., Madau P., Zemp M., Kuhlen M., Quilis V., 2009, *MNRAS*, 398, L21
 Steinmetz M., White S. D. M., 1997, *MNRAS*, 288, 545
 Yurin D., Springel V., 2014, *MNRAS*, 444, 62

This paper has been typeset from a $\text{\TeX}/\text{\LaTeX}$ file prepared by the author.